P1.58 Detection of electrification with the co-to-cross correlation coefficient with storm microphysics analysis

J.C. Hubbert[1]*, W. Deierling[1] and P. Kennedy[2]

[1]National Center for Atmospheric Research, Boulder, CO
[2]Colorado State University, Fort Collins, CO

1. Introduction

As convective storms develop and become electrified, typically many ice crystals are produced. These ice crystals can become aligned by the electric field and obtain a mean canting angle that is away from the horizontal. Without electrification, ice crystals will align themselves horizontally due to aerodynamic forces, unless the ice crystals are very small ($<$ 30 microns with Brownian motion). If these ice crystals are in high enough concentrations, polarimetric radar can detect them with several variables. Previous authors have identified canted ice crystals with ϕ_{dp} (differential phase) and LDR (Linear Depolarization Ratio). Here we demonstrate how these ice crystals are detected using the ρ_x (co-to-cross correlation coefficient) . Using ρ_x, ϕ_{dp}, LDR and Z_{dr}, inferences about the ice microphysics and cloud electrification can be made. Experimental measurements from S-Pol, NCAR's (National Center of Atmospheric Research) S-band polarimetric radar are given that illustrate the theoretical analysis. The data set and analysis is further augmented with data from the Colorado LMA (Lightning Mapping Array) maintained by Colorado State University. A radar scattering model as well as T-matrix scattering simulations are used to explain the observed polarimetric signatures.

2. Modeling $\rho_{\mathbf{hhvh}}$ and $\rho_{\mathbf{vvhv}}$

There are two co-to-cross correlation coefficients (ρ_x), namely ρ_{hhvh} and ρ_{vvhv}, where the subscript pairs describe the two times series of the covariance. For example the subscript hhvh means (from right to left) 1) the transmit h receive v times series and 2) the transmit h receive h time series. When necessary we will refer to specific co-to-cross correlation but will use ρ_x for general discussions. The model used is described in (Hubbert et al. 2014a,b; Hubbert and Bringi 2003). The T-matrix method is used to calculate the 2×2 scattering matrix. The model then integrates over the specified size and orientation distributions and creates the 3×3 covariance matrix. The experimental PSD (particle size distribution) used here is a combination of ice crystals (ice columns) and graupel and is described in Hubbert et al. (2014a). The ice columns are modeled with and AR (axis ratio) of 2 and a maximum diameter (equivalent spherical) of .625 mm and the plane containing the mean major and minor axes is perpendicular to the radar line of sight. The standard deviation of the canting angles is $10°$. When the mean canting angle is zero, the Z_{dr} and LDR are 2.7 dB and -29.3dB, respectively. Graupel is modeled as having a uniform random spatial distribution with an axis ratio of 0.8 and a density of 0.3g/cm^3 yielding a LDR of -37.6 dB. These two PSDs are then combined with the reflectivity of the graupel exceeding that of the ice crystals by 10 dB. When the mean canting angle is zero, the Z_{dr} and LDR are 0.19 dB and -35 dB. Since forward scattering is coherent (Bringi and Chandrasekar 2001) the propagation medium is completely characterized by the differential phase in the particles' eigenpolarization basis. The eigenpolarization basis is that coordinate system where K_{dp} is maximized. For example, using the ice crystal distribution above, if the mean canting angle of crystals is $0°$ (relative to earth) then H-V polarization basis (perpendicular to the direction of propagation) would then define the eigen-basis. If the mean canting angle of the PSD is changed, the eigen-basis K_{dp} remains unchanged. Thus, if the PSD were give a mean canting angle of $45°$, the observed (H-V basis) K_{dp} would be zero but the principal plane K_{dp} remains the same as it was when the mean canting angle was $0°$. As shown below, the magnitude of the ρ_{hhvh} and ρ_{vvhv} is a very strong function of the amount of accumulated principal plane ϕ_{dp}.

If the mean canting angle of the PSD is zero (and the canting angles are symmetrically distributed around the mean) then $\rho_{hhvh} = \rho_{vvhv} = 0$ independent of principal plane ϕ_{dp}. There will be cross coupling at backscatter due to the distribution of the canting angles and this will give LDR a finite value (-29.3 dB for the above ice crystals).

The co-to-cross correlation coefficient has been addressed in Hubbert and Bringi (2003) and in Ryzhkov et al. (2002). In Hubbert and Bringi (2003) the modeled PSD came from a single particle type (rain). Here we model ρ_{hhvh} and ρ_{vvhv} for a combination of two particle types: aligned ice crystals and randomly oriented graupel

*NCAR/EOL, Boulder, Colorado 80307, email: hubbert@ucar.edu

as was done in Hubbert et al. (2014a).

Figure 1 shows ρ_{hhvh} and ρ_{vvhv} for the two-population mixture as a function of the mean backscatter canting angle. There are no propagation effects. At $0°$ and $90°$ mean canting angle, the ρ_{hhvh} and ρ_{vvhv} are zero (Bringi and Chandrasekar 2001). As the mean canting angle increases, both ρ_{hhvh} and ρ_{vvhv} increase. The maximum ρ_{hhvh} occurs at about $30°$ and the maximum ρ_{vvhv} occurs at about $60°$ but the increase in correlation from $45°$ is insignificant. *Most importantly, the maximum correlation never exceeds 0.25 for this mixture.*

As discussed in Hubbert et al. (2014a), many times in the ice phase of convective storms there are aligned ice crystals as evidenced by an observed significant increase (decrease) in ϕ_{dp}. If the scattering medium consisted of only the aligned ice particles that gave rise to the ϕ_{dp} increase (decrease), then there would be significant Z_{dr} value (say $|Z_{dr}| > 1$ dB). However, most of the time Z_{dr} is close to zero. As argued in Hubbert et al. (2014a), this indicates the presences of ice particles (e.g., graupel) that have a more random spatial orientation distribution (polar metrically isotropic) such that their Z_{dr} is close to zero and with reflectivity much greater than the ice crystals (such as the present mixture). For such mixtures of ice crystals and graupel, if high values of ρ_{hhvh} and ρ_{vvhv} are observed (i.e.$>$ 0.25) this indicates that propagation effects are the cause of the high ρ_x, which is demonstrated next.

Figure 2 shows ρ_{hhvh} and ρ_{vvhv} for the two-population mixture as a function of the principal plane ϕ_{dp} with the mean canting angle of the ice crystals as a parameter. Both the propagation and backscatter medium have the same mean canting angle. For larger canting angles, say $> 20°$, only about $3°$ of ϕ_{dp} accumulation is needed to drive the correlation to about the 0.5 level.

Figure 3 is similar to Fig. 2 but with the reflectivity of the graupel 2 dB higher than that of the ice crystals. Thus, as the reflectivity of the ice crystals increases relative to the graupel, the ρ_{hhvh} and ρ_{vvhv} become higher as compared to Fig. 2.

Figure 4 is similar to Fig. 2 except the backscatter medium has a mean canting angle of $0°$ and only the mean canting angle of the propagation medium is the parameter. Interestingly, for the larger canting angles, $> 20°$ the correlations increase very rapidly as the principal plane ϕ_{dp} increases. Only a degree or two increase in ϕ_{dp} causes the correlation to exceed 0.5. In general, if the LDR of the graupel is decreased, this increase in correlation is even more rapid. *If $LDR = -\inf$ dB, then theoretically any increase in ϕ_{dp} causes both ρ_{hhvh} and ρ_{vvhv} to be 1.* Additionally, since this increase in ρ_x is a propagation effect, the ρ_x will remain high out along that radial thus causing radial stripes of elevated ρ_x. This is frequently observed and is similar to the streaks in SHV (simultaneous H and V transmit) Z_{dr}.

The two phases, ϕ_{hhvh}, ϕ_{vvhv} of the co-to-cross correlations are shown in Fig. 5 as a function of principal plane ϕ_{dp} with the mean canting angle of the scattering medium (both propagation and backscatter) as a parameter. The phase of the co-to-cross correlations have been discussed before (Hubbert and Bringi 2003; Ryzhkov et al. 2002) where it was established that

$$\phi_{dp} = \phi_{vvhv} - \phi_{hhvh} \quad (1)$$

The co-to-cross phases corresponding to Fig. 2 are shown in Fig. 5. After a few degrees of principal plane ϕ_{dp}, all curves approach $+90°$ or $-90°$. For mean canting angles between $0°$ and $90°$, ϕ_{hhvh} is negative while ϕ_{vvhv} is positive. For mean canting angles between $0°$ and $-90°$, ϕ_{hhvh} is positive while ϕ_{vvhv} is negative. This then suggests that the sign of the canting angle of the ice crystals can be determined from the sign of the co-to-cross phases. Also, if the co-to-cross phase can be estimated accurately, the mean canting angle can be determined from the crosspolar optimum polarizations (Hubbert and Bringi 1996; Hubbert et al. 1998).

3. Experimental Data

The following radar data was gathered by S-Pol on 22 May 2014. The initiation and growth of a small convective cell was captured with PPI and RHI scans over a 2 hour time period. The electrical activity was captured by the Colorado LMA. We present a data set that shows the polarimetric signatures before the first LMA detected lightning strike. Thus we examine if polarimetric radar can detect charged aligned ice particles before the first electrical discharge.

Shown in Figures 6 and 7 are discharge source points as a function of time (top panels) and in space (the three other color panels). The top panel of Fig. 6 shows the source points of the first flash occurring at about 17:31:42 UTC. The colors mark the time of occurrence. The other panels show the source points projected on the horizontal plane and the two vertical side planes. Similarly, Figure 7 shows the source points for the entire life of the convective cell, 17:31 to 19:23 UTC.

Figure 8 shows the reflectivity of the convective cell at 17:19 UTC at $2.5°$ elevation angle. The highest reflectivity is about 35 dBZ. The yellow line shows the approximate location of the following RHI cuts. Distances are in km from S-Pol. Figures 9 to 14 show RHIs of the radar variables gathered at 17:19:38 UTC, or about 11 minutes before the first observed lightning. From Figure 9 the maximum reflectivities are less than 40 dBZ. Figure 10 shows ρ_x with white ovals marking where elevated ρ_x is very likely due to canted ice crystals, and another oval, marked as "artifact", where elevated ρ_x is likely due to sidelobe ground clutter. The ovals are overlaid on the other radar variable plots. It is instructive to compare the radar variables in the two ovals so that a "good" (i.e., caused by canted ice crystals) ρ_x signature can be contrasted to a "bad" one. The Z_{dr} in Fig. 11 shows that the good Z_{dr} data is spatially smooth while the bad data show spatial variability. The cross-channel SNR is shown in Fig. 10. The good data has SNRs from 3 to 10 dB, which is sufficient to yield reliable ρ_x, whose value is controlled by the precipitation particles in the resolution volume. The bad data shows much higher SNRs so that by SNR alone, good and bad data regions cannot be separated. Figure 13 shows that "good" ϕ_{dp} is spatially smooth while the bad data is quite noisy. Figure 14 shows LDR being quite low (mostly < -30 dB) in the good region while LDR is very high in the bad region. The high LDR is likely caused by sidelobe ground clutter. From these plots, reliable elevated ρ_x that marks canted ice crystals can be identified by $\rho_x > 0.4$, cross-channel SNR$>$ 2 dB, LDR< -25 dB, and spatially smooth ϕ_{dp} and Z_{dr}.

In this example ρ_x is sensitive to the canted ice crystals while neither ϕ_{dp} nor LDR show evidence of aligned canted ice crystals. Typically we have observed that for electrified storms, increasing, decreasing or both radial streaks of ϕ_{dp} are seen. In this case, the convective cell is quite small and sufficient concentrations of aligned ice crystals are not present to produce an observable phase shift in ϕ_{dp} whereas the canted ice crystals cause sufficient depolarization to increase ρ_x to the observed values. The ice crystals could have a mean canting angle near $45°$ so that no change in ϕ_{dp} versus range would be observed. The depolarized signal caused by the canted ice crystals could also increase LDR. In this case, however, apparently the polarimetrically isotropic particles (e.g., graupel) mask the LDR signature of of the canted ice crystals. Thus, ρ_x marks the region of canted ice crystals before any other radar variable and importantly, 11 minutes before any occurrence of lightning.

Another data example is shown in Figs. 15 to 17. The white overlay contours indicate source points from the LMA. This data example is from a convective cell which is more mature (larger and more electrically active) than the previous case. Figure 16 shows ϕ_{dp} with both increasing (yellow color scale) and decreasing (pink color scale) regions. The interpretation is that the positive region contains ice crystals that are oriented more horizontally while in the second region, the ice crystals are oriented more vertically. The ρ_x in Fig. 17 shows a large red stripe that corresponds to the region in ϕ_{dp} in between the increasing and decreasing regions. This would indicate that the ice crystals in this region are oriented more closely to $45°$ so that maximum depolarization is occurring thus increasing ρ_x. Interestingly, the white contours connect the regions of increasing and decreasing ϕ_{dp}. This data example is offered to demonstrate the possible microphysical interpretation from such data sets.

4. Summary and Conclusions

In this paper cross-coupling of H and V waves, due to canted ice crystals, was simulated and analyzed, and experimental S-Pol data was given to illustrate the theory. Microphysical interpretations were offered. The co-to-cross correlation coefficient, ρ_x, was modeled for a PSD consisting of both ice crystals (columns) and graupel where the reflectivity due the graupel was 2 dB and 10 dB higher than the ice crystal reflectivity. Modeling showed that if the intrinsic LDR of the graupel was $-\inf$ dB, only a very small amount of depolarization due to canted ice crystals needed to occur in order to increase ρ_x to high levels (> 0.9), provided the SNR of the cross channel is high. The data example given showed that ρ_x detected oriented ice crystals 11 minutes before the first occurrence of lightning as measured by the Colorado LMA. Neither ϕ_{dp} nor LDR showed evidence of aligned ice crystals at that point in time. ρ_x is more sensitive to canted ice crystals than LDR since the two time series that are in ρ_x have uncorrelated noise, whereas LDR is a power (zero-lag) auto correlation product. A further data example showed the potential for microphysical interpretation when polarimetric radar data, with ρ_x available, is combined with LMA data.

Acknowledgment We thank Dr. William Rison (New Mexico Institute of Mining and Technology) for the reprocessed Colorado LMA lightning data. The National Center for Atmospheric Research is sponsored by the National Science Foundation. Any opinions, findings and conclusions or recommendations expressed in this publication are those of the authors and do not necessarily reflect the views of the National Science Foundation.

References

Bringi, V. and V. Chandrasekar, 2001: *Polarimetric Doppler Weather Radar*. Cambridge Univ. Press, Cambridge, UK.

Hubbert, J. and V. Bringi, 1996: Specular null polarization theory: Applications to radar meteorology. *IEEE Trans. Geosci. Remote Sensing*, **34**, 859–873.

— 2003: Studies of the polarimetric covariance matrix: Part II: Modeling and polarization errors. *J. Atmos. Oceanic Technol.*, 1011–1022.

Hubbert, J., V. Bringi, L. Carey, and S. Bolen, 1998: CSU-CHILL polarimetric radar measurements in a severe hail storm in eastern Colorado. *J. App. Meteor.*, **37**, 749–775.

Hubbert, J., S. Ellis, W.-Y. Chang, M. Dixon, and Y.-C. Liou, 2014a: X-band polarimetric observations of cross-coupling in the ice phase of convective storms in taiwan. *J. of Applied Meteor. and Clim.*.

Hubbert, J., S. Ellis, W.-Y. Chang, S. Rutledge, and M. Dixon, 2014b: Microphysical interpretation of S-band simultaneous horizontal and vertical polarization transmit radar data. *J. of Applied Meteor.and Clim.*.

Ryzhkov, A., D. Zrnić, J. Hubbert, V. Bringi, J. Vivekanandan, and E. Brandes, 2002: Polarimetric radar observations and interpretation of co-cross-polar correlation coefficients. *J. Atmos. Oceanic Tech.*, **19**, 340–354.

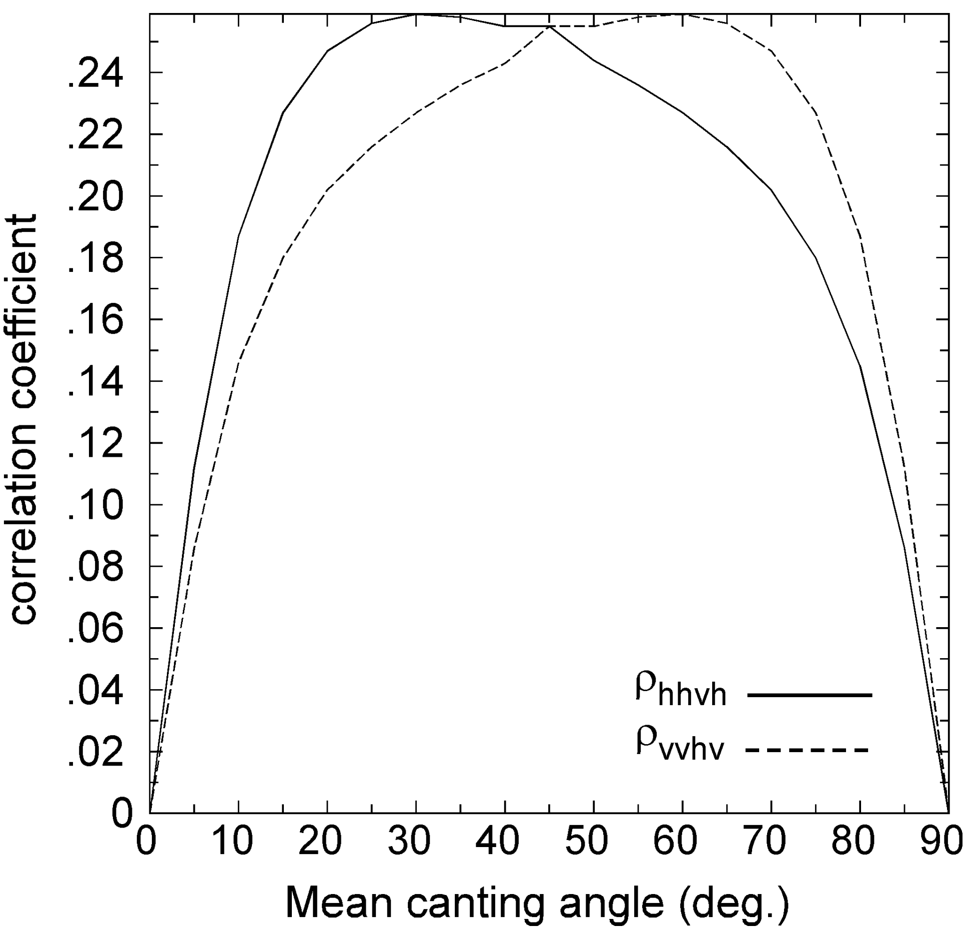

Figure 1: *The co-to-cross correlation coefficient as a function the mean canting angle of the backscatter medium.*

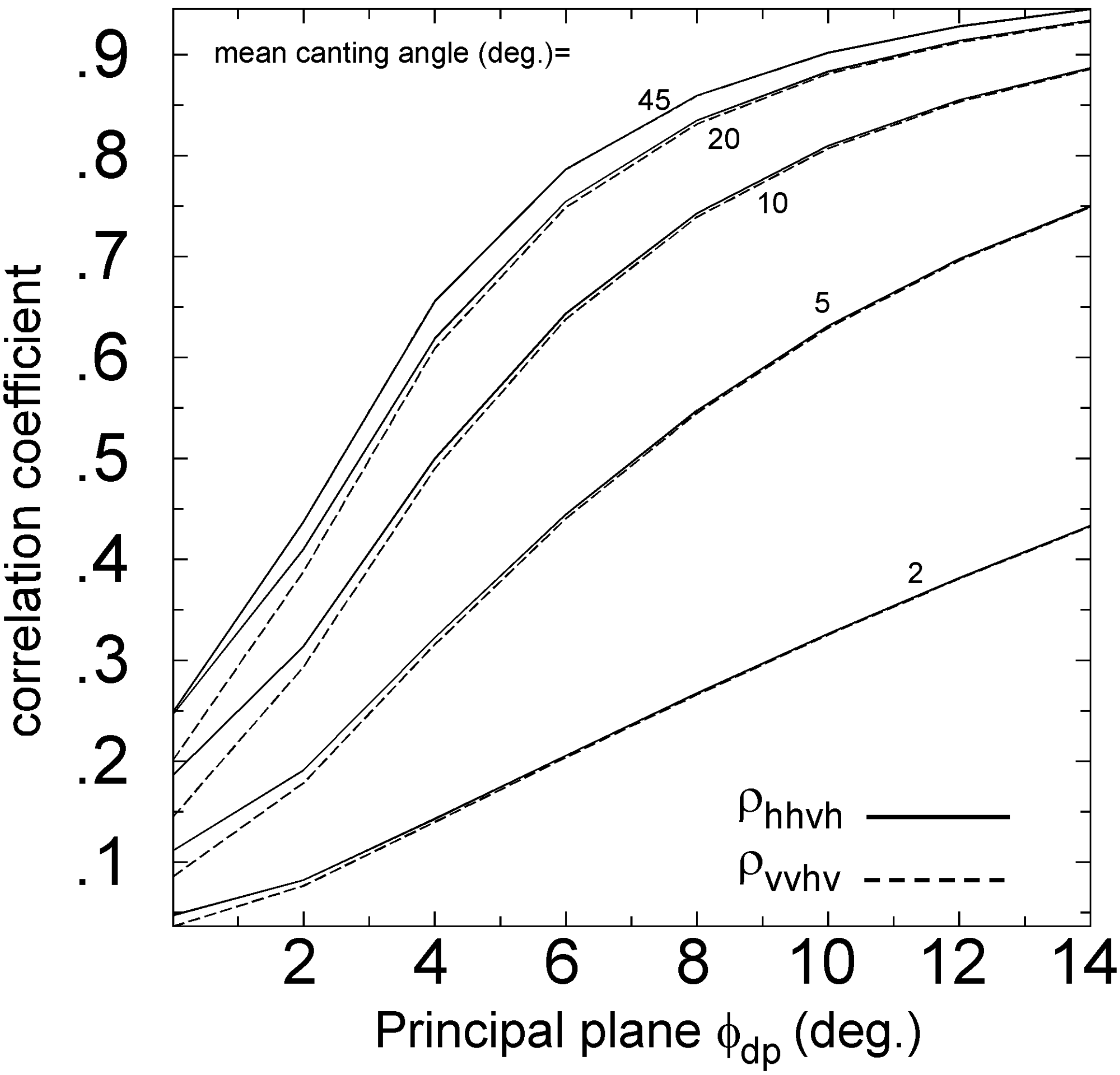

Figure 2: *The co-to-cross correlation coefficients, ρ_{hhvh}, ρ_{vvhv} as a function of the principal plane ϕ_{dp} with the mean canting angle of the medium (both the propagation and backscatter) as a parameter. The scattering medium is composed of both ice crystals and graupel with the the graupel's reflectivity 10 db higher than the ice crystal's reflectivity.*

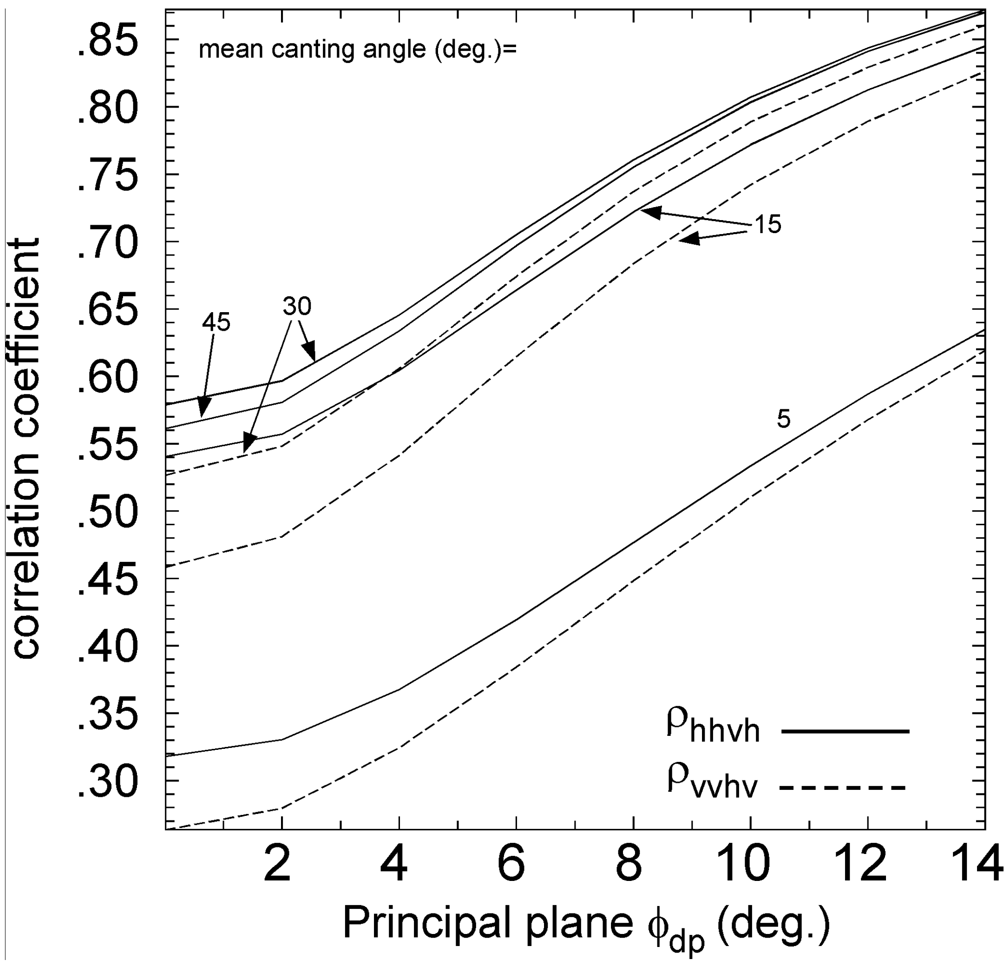

Figure 3: *Similar to Fig. 2 except the graupel's reflectivity is 2 db higher than the ice crystal reflectivity.*

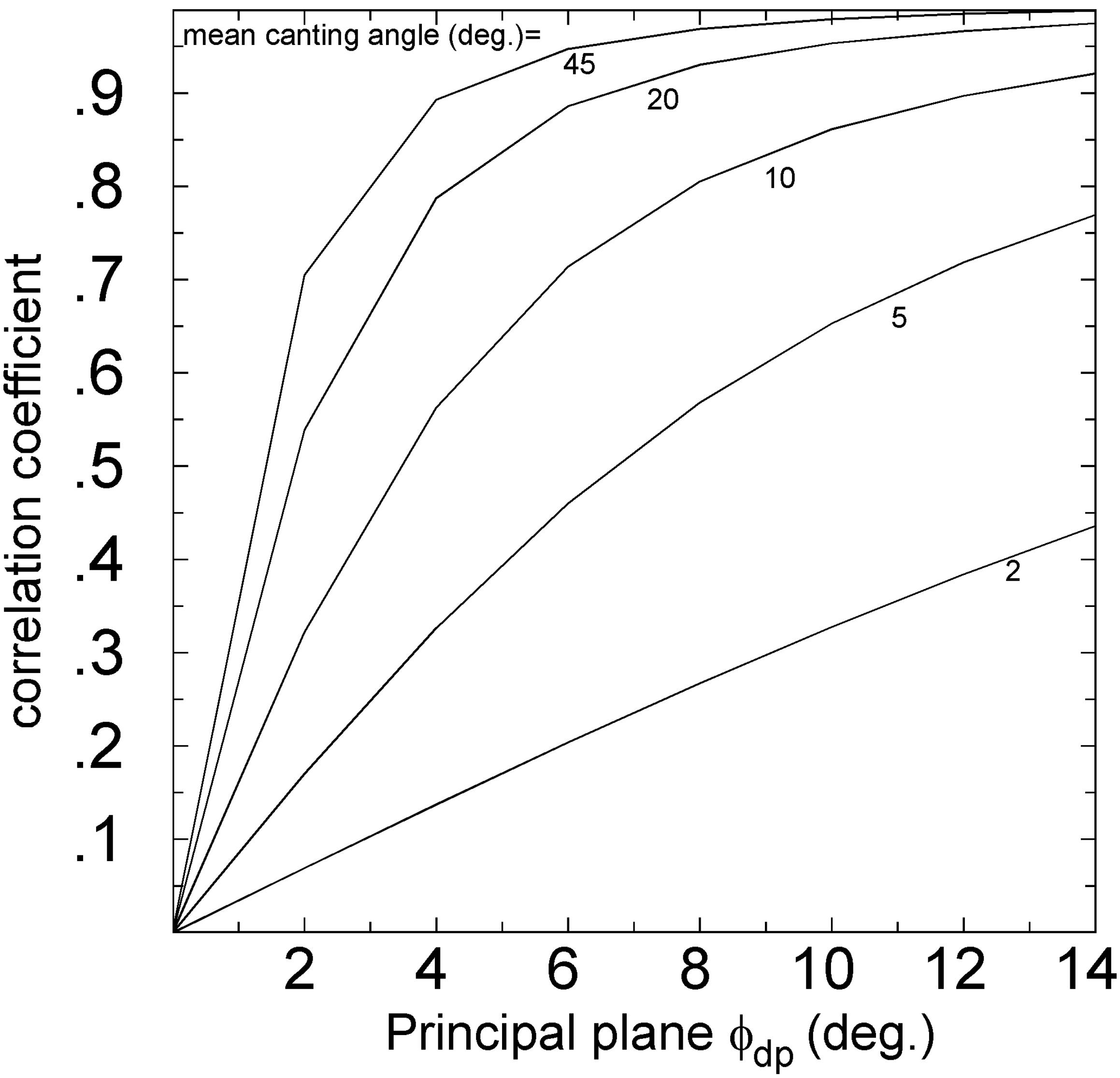

Figure 4: *Similar to Fig. 2 except the backscatter medium's mean canting angle is zero.*

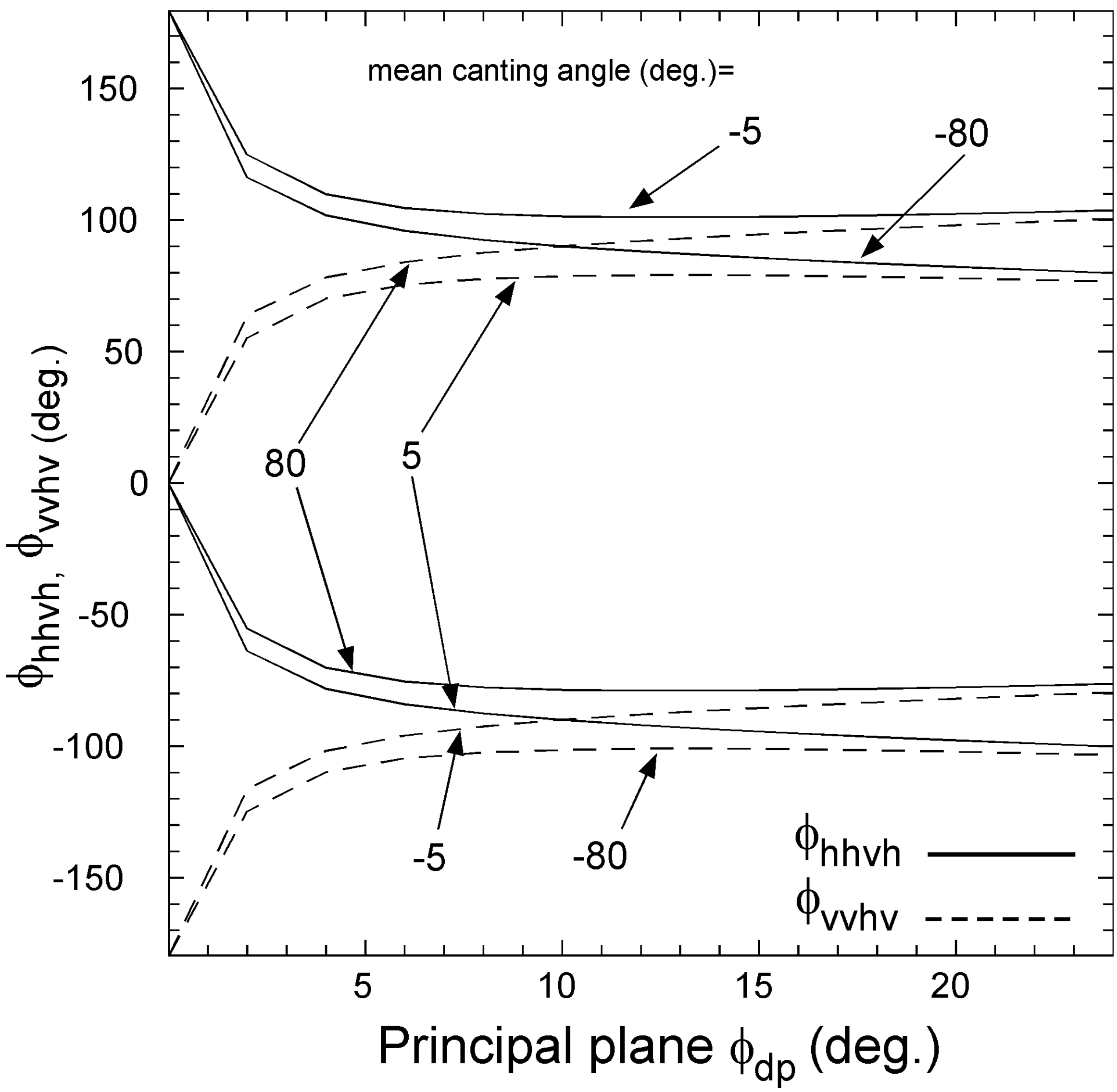

Figure 5: *For the same PSD as in Fig. 2. The two co-to-cross differential phases corresponding to* ρ_{hhvh} *and* ρ_{vvhv}.

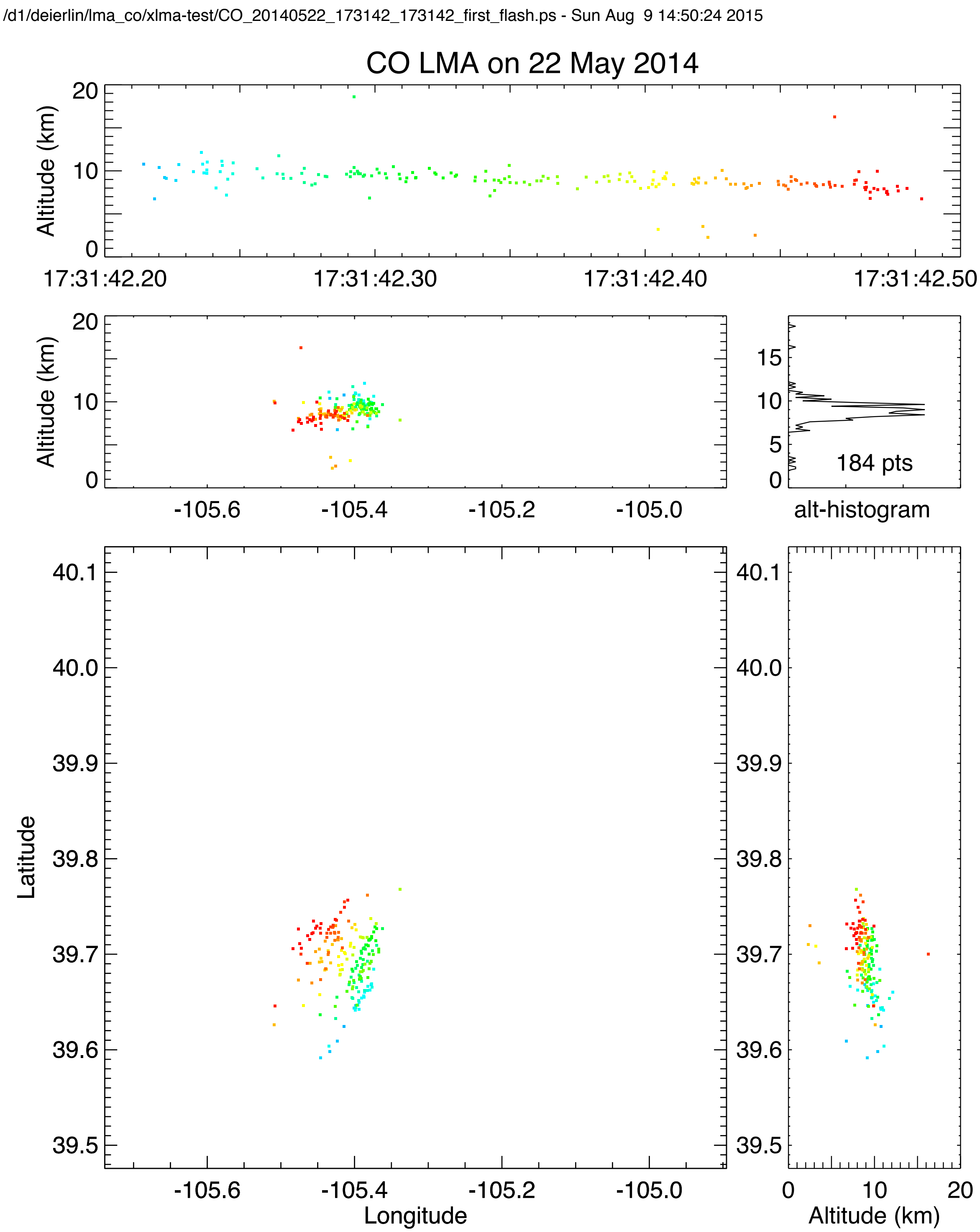

Figure 6: *LMA source point diagram for the first lightning discharge on 22 May 2014.*

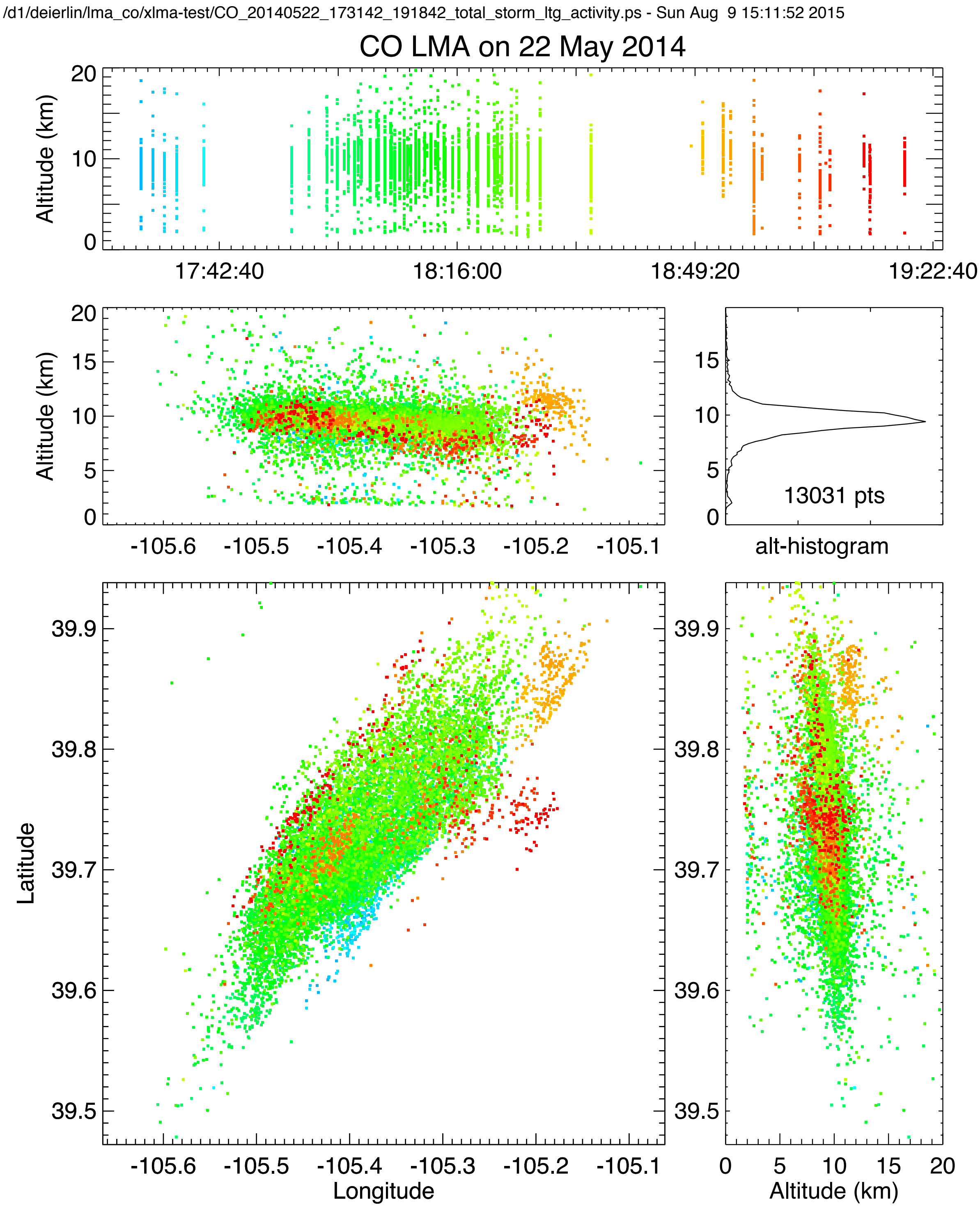

Figure 7: *LMA source point diagram for the life cycle of the cell on 22 May. 2014.*

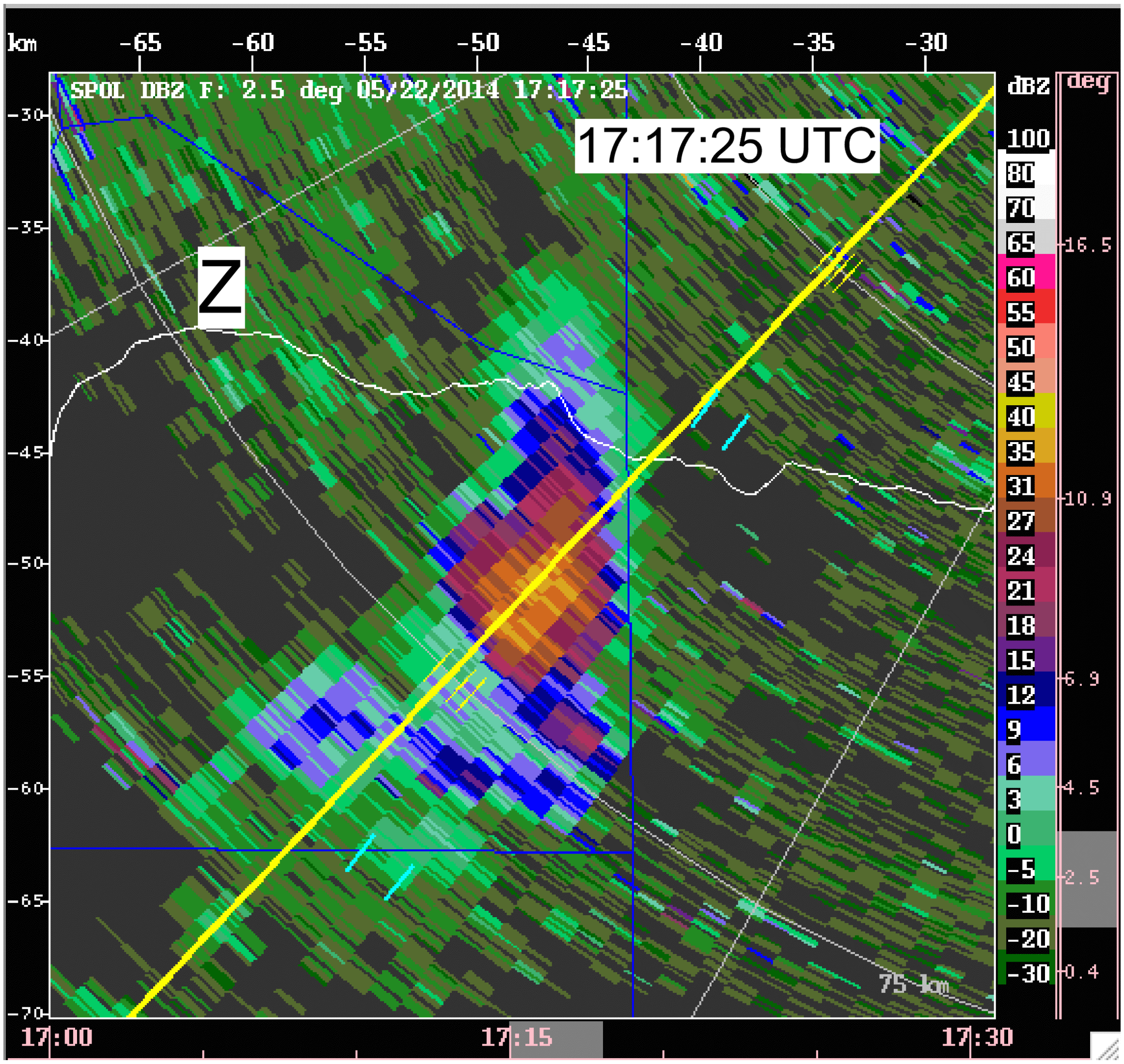

Figure 8: *An PPI of S-Pol Reflectivity showing the small convective cell at the location of the RHIs shown at 17:17:25 UTC.*

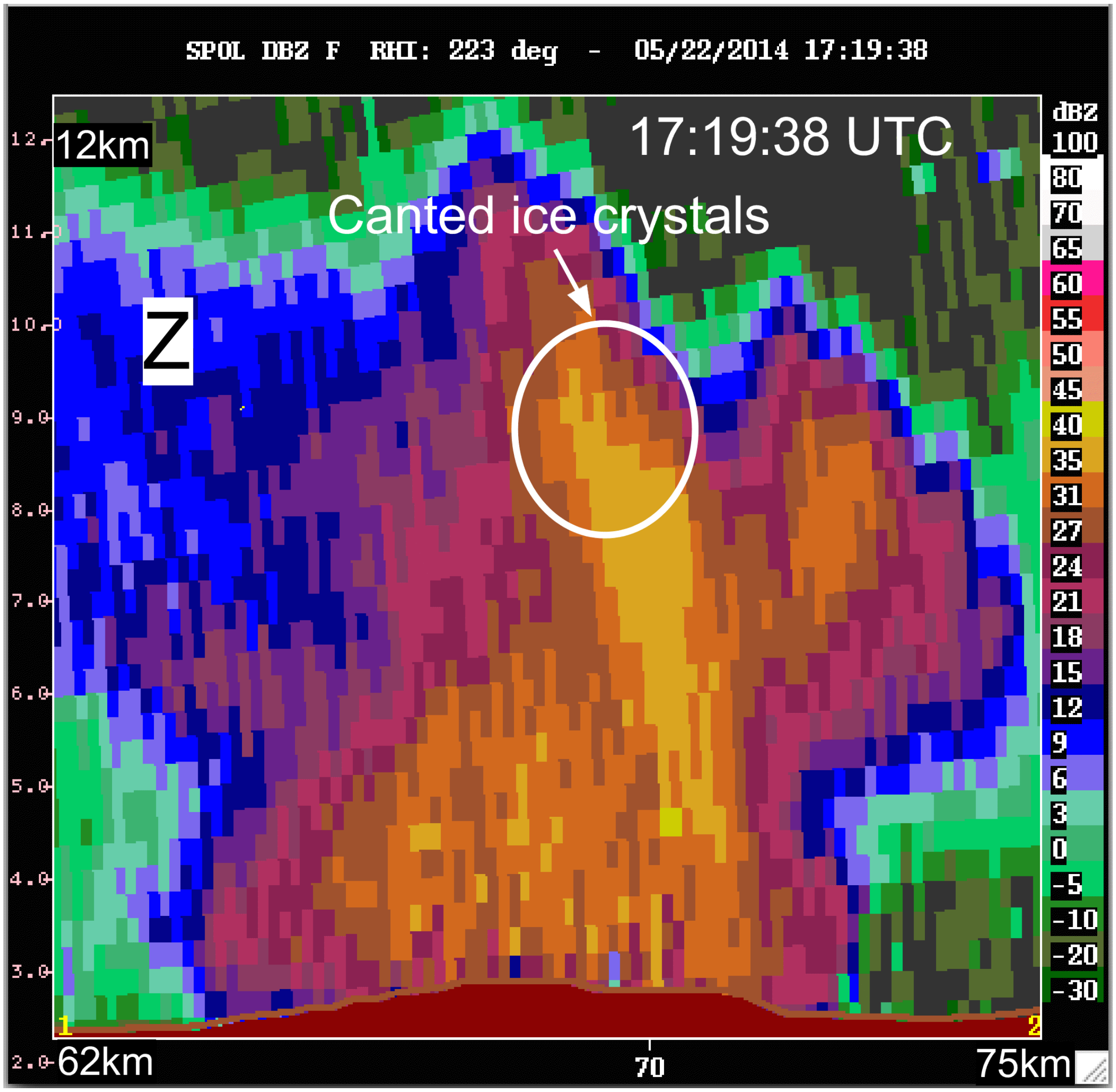

Figure 9: *An RHI of S-Pol Reflectivity. White circle show location of canted ice crystals.*

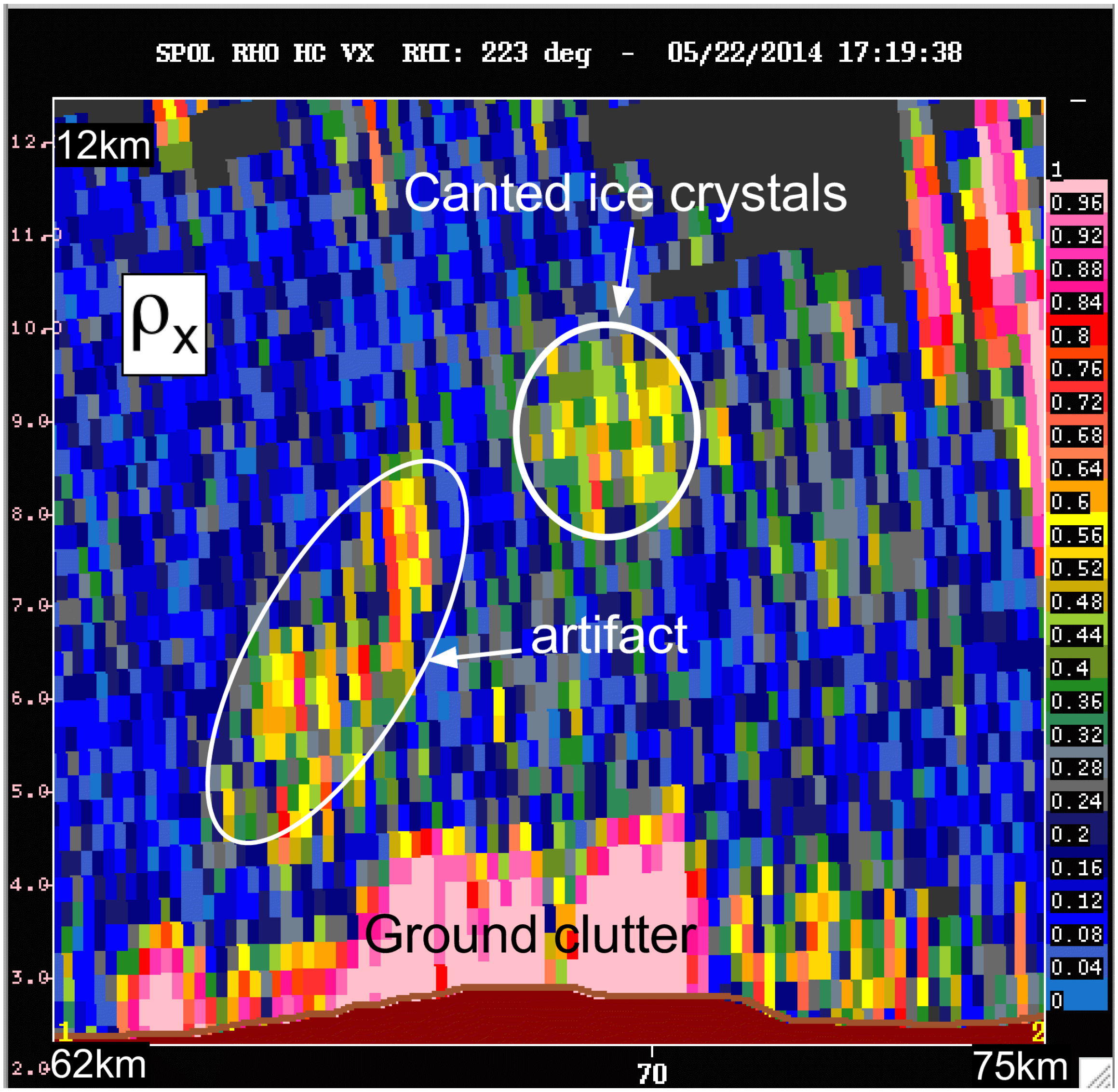

Figure 10: *An RHI of S-Pol co-to-cross correlation coefficient, ρ_x.*

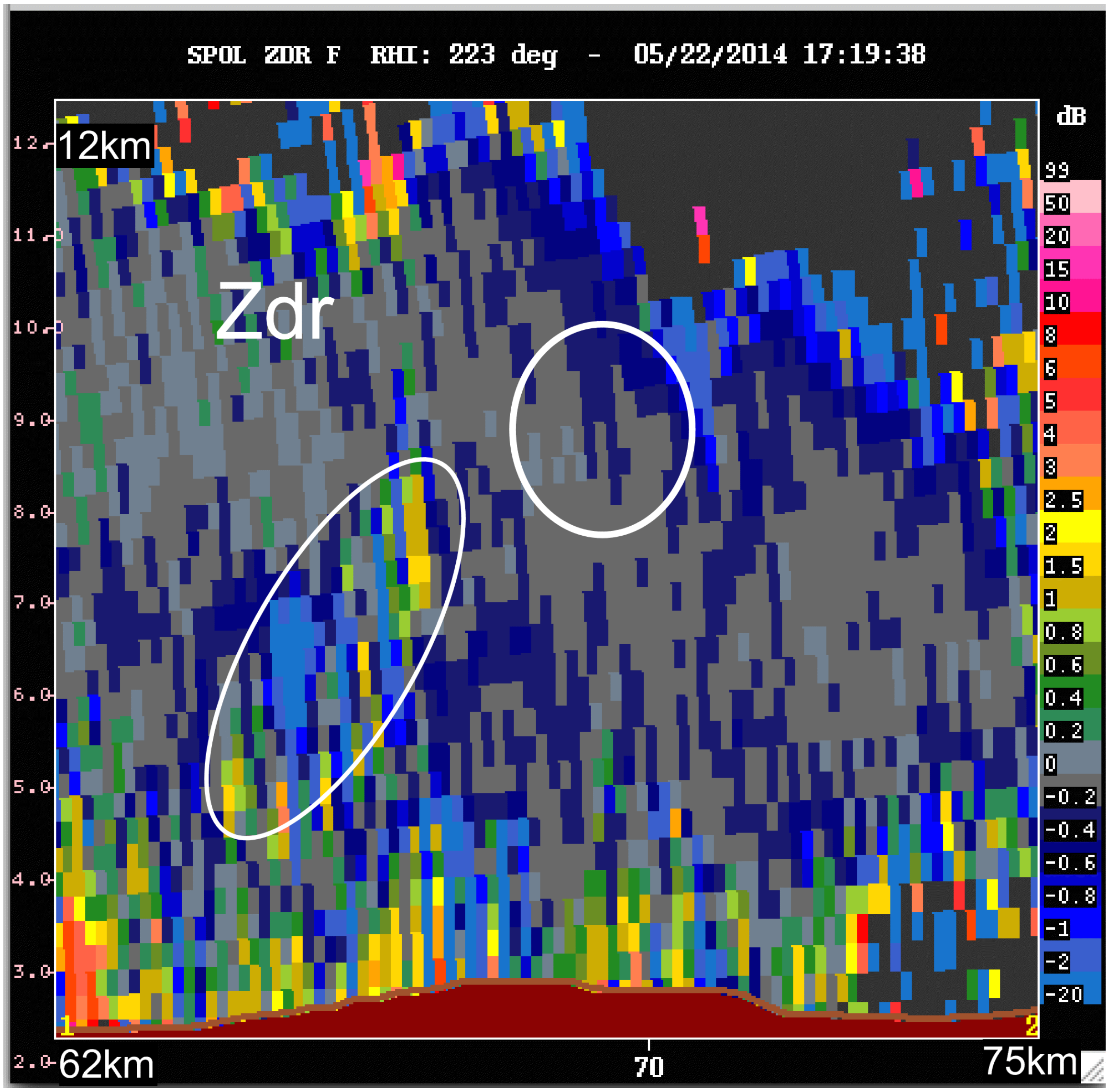

Figure 11: *An RHI of S-Pol* Z_{dr} .

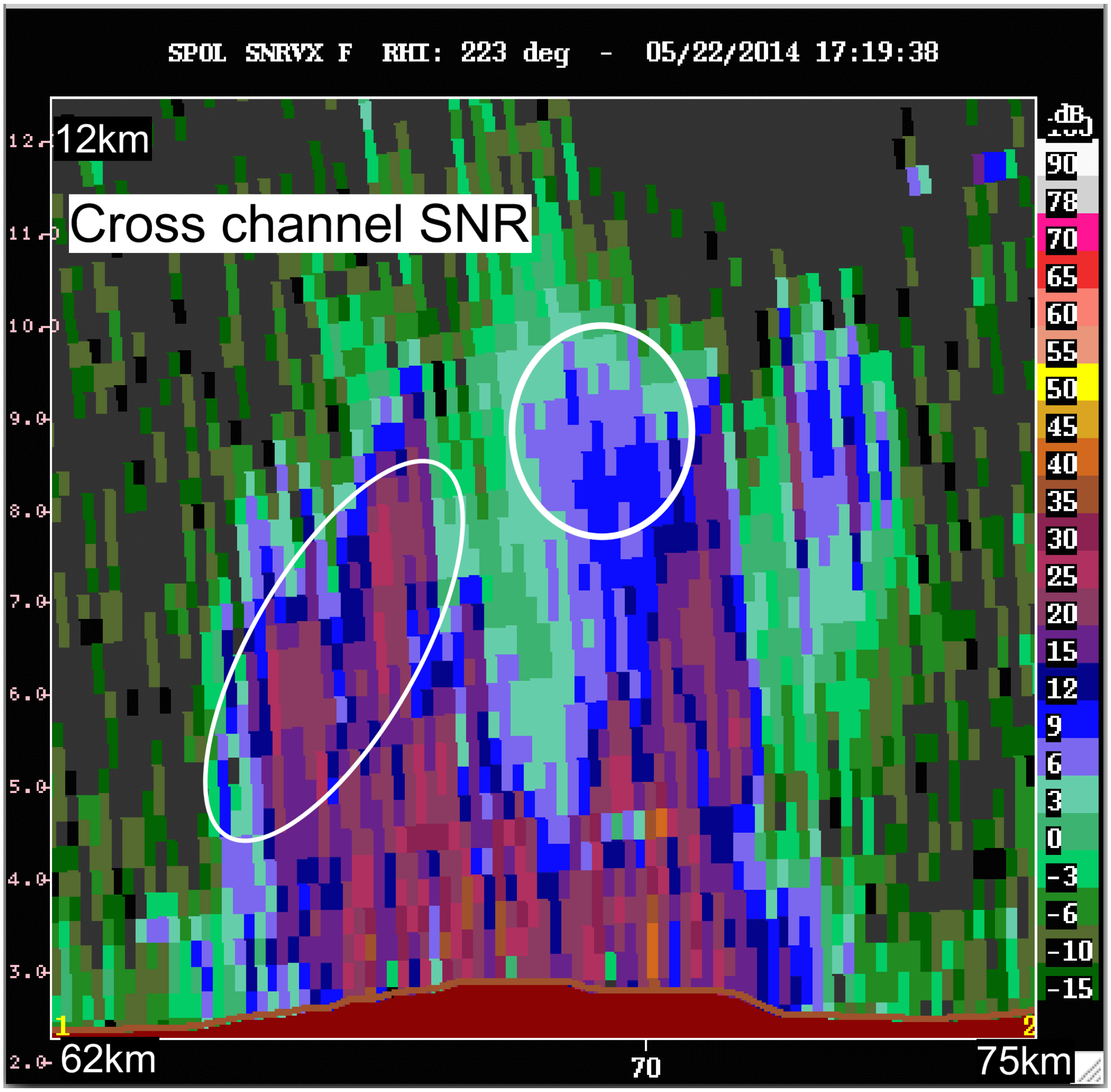

Figure 12: *An RHI of S-Pol cross channel SNR.*

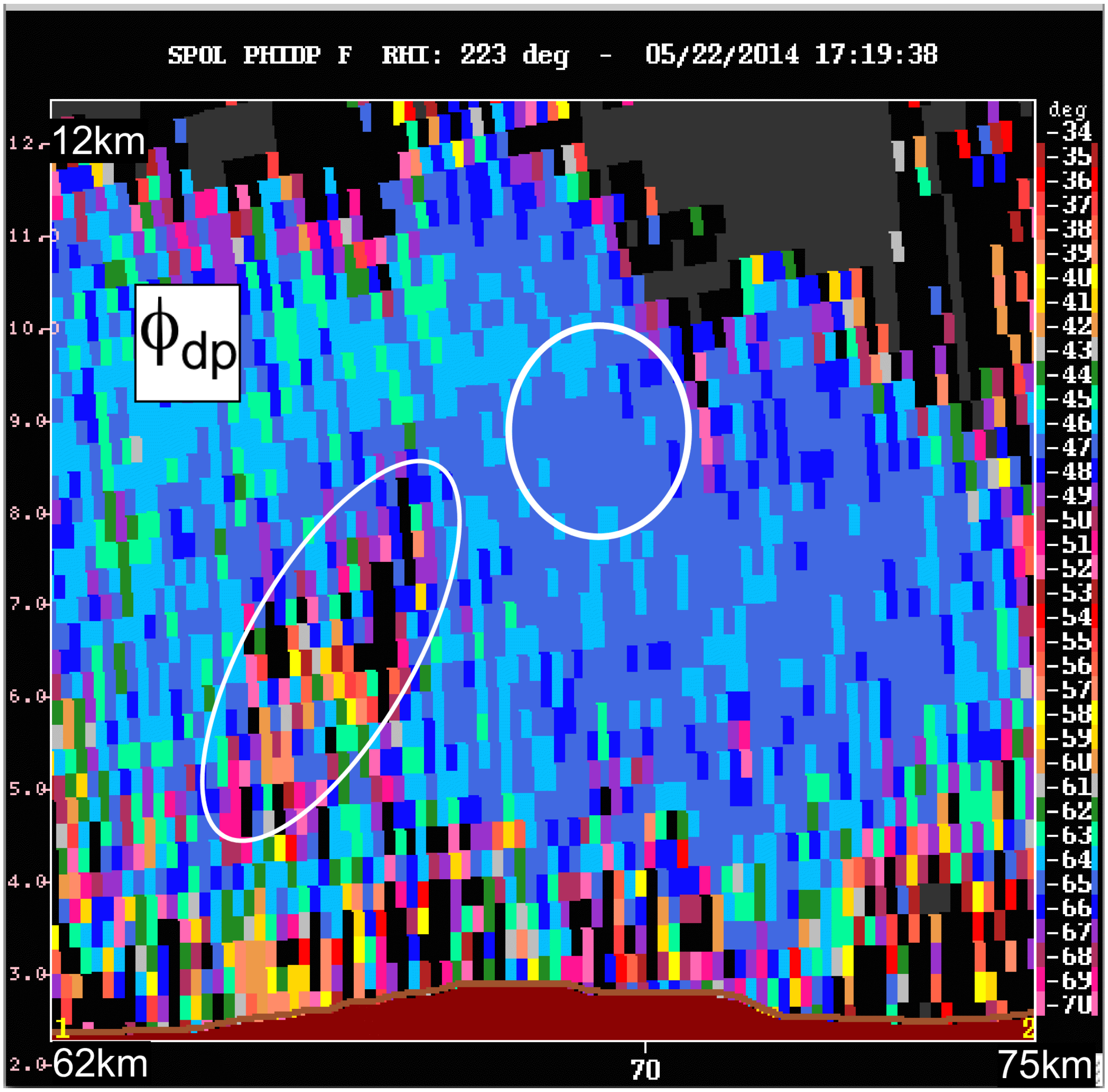

Figure 13: *An RHI of S-Pol* ϕ_{dp} .

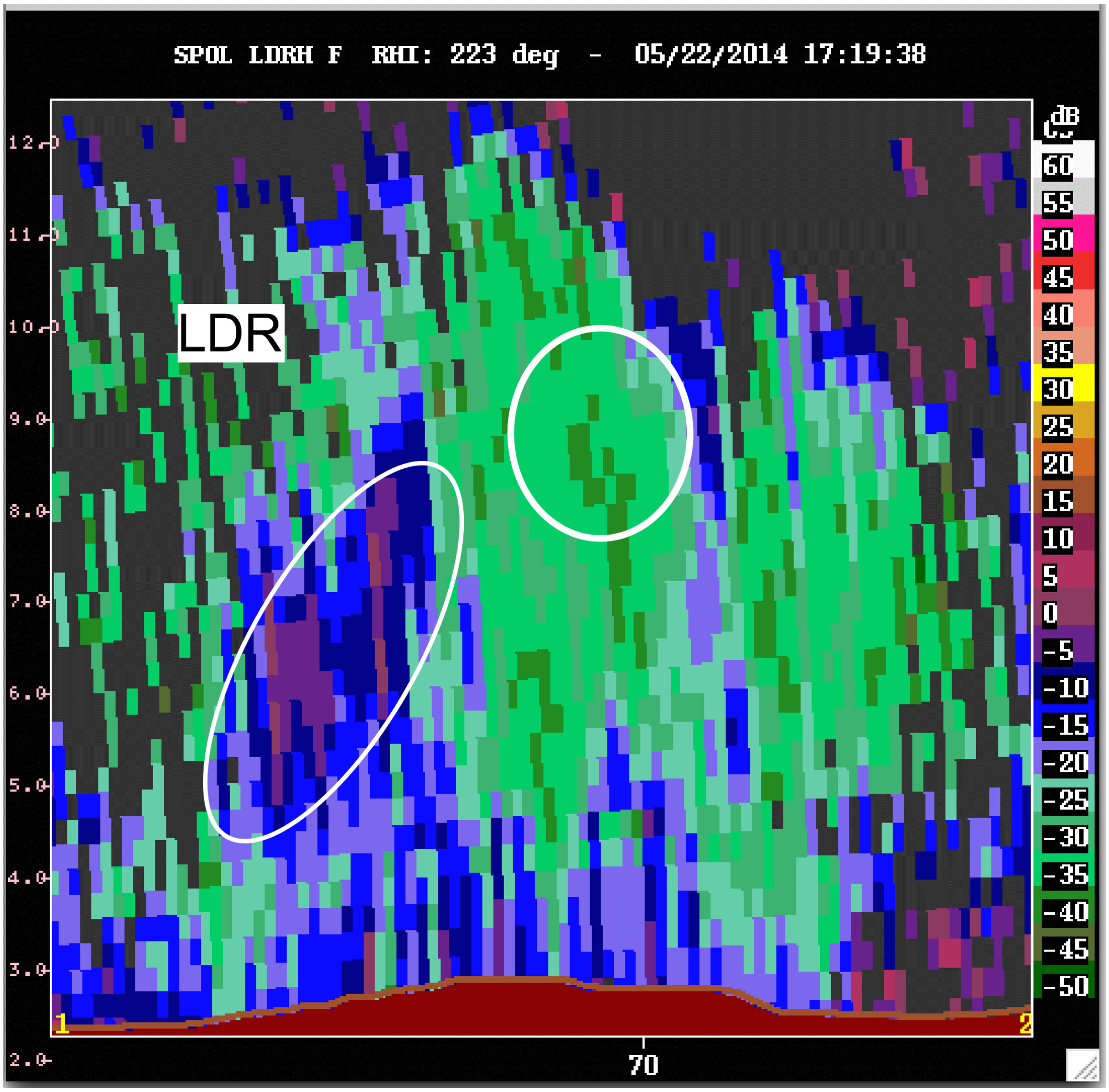

Figure 14: *An RHI of S-Pol LDR.*

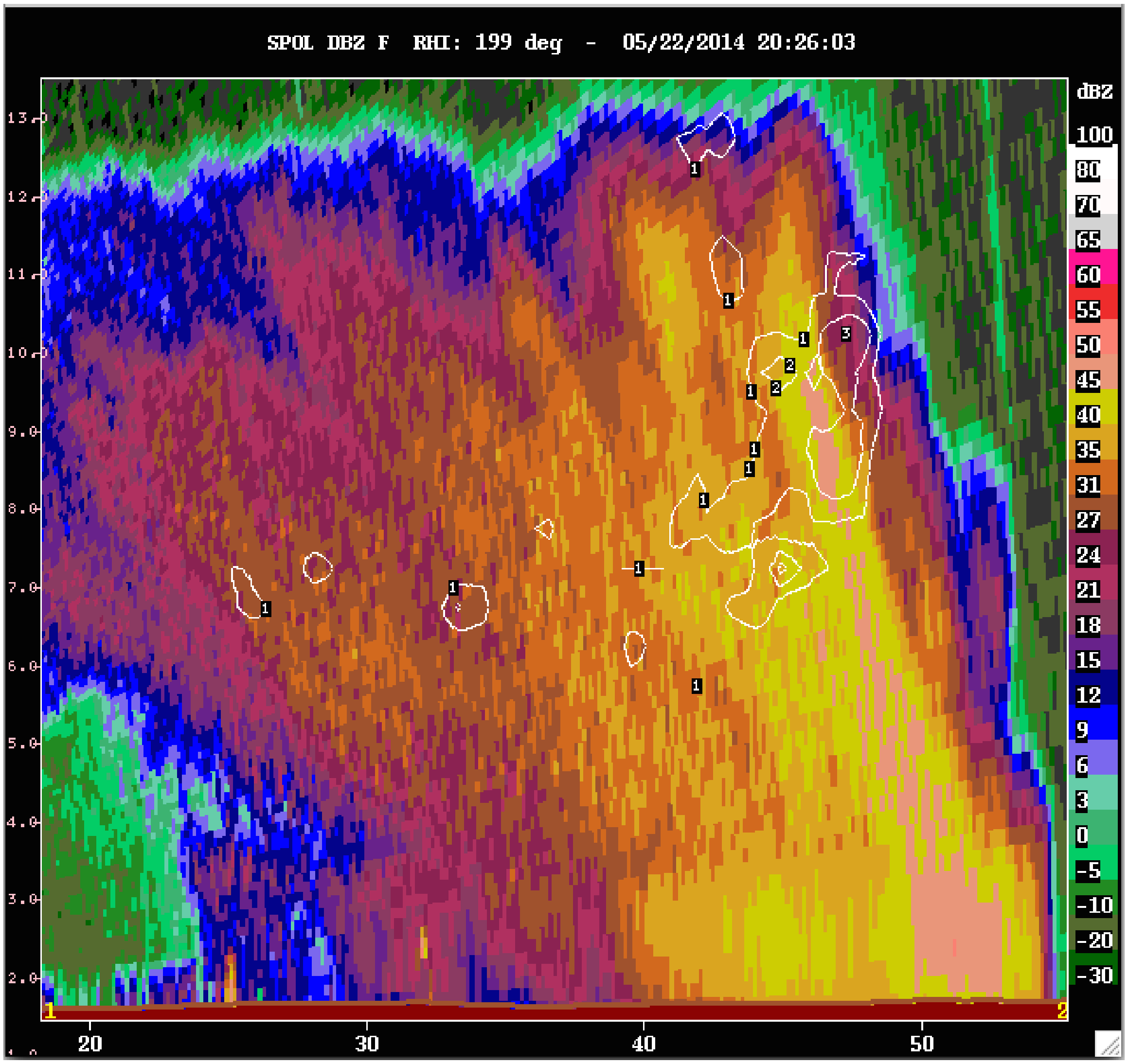

Figure 15: *An RHI of S-Pol Reflectivity from 22 May 2014 at 20:26:03 UTC. The white contours lines demark source points from the LMA from 20:24 to 20:26 UTC.*

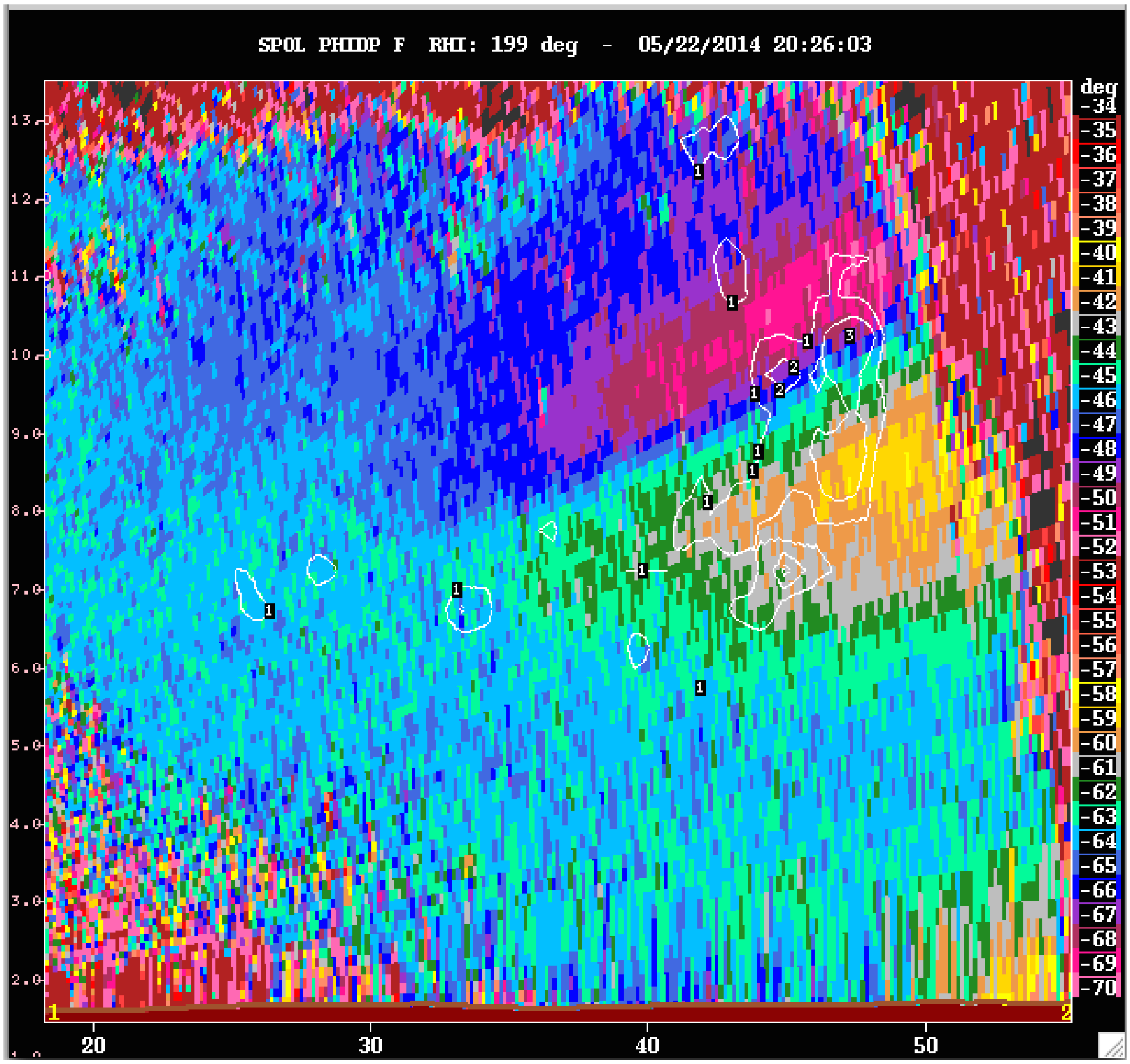

Figure 16: *An RHI of S-Pol ϕ_{dp} accompanying Fig. 15.*

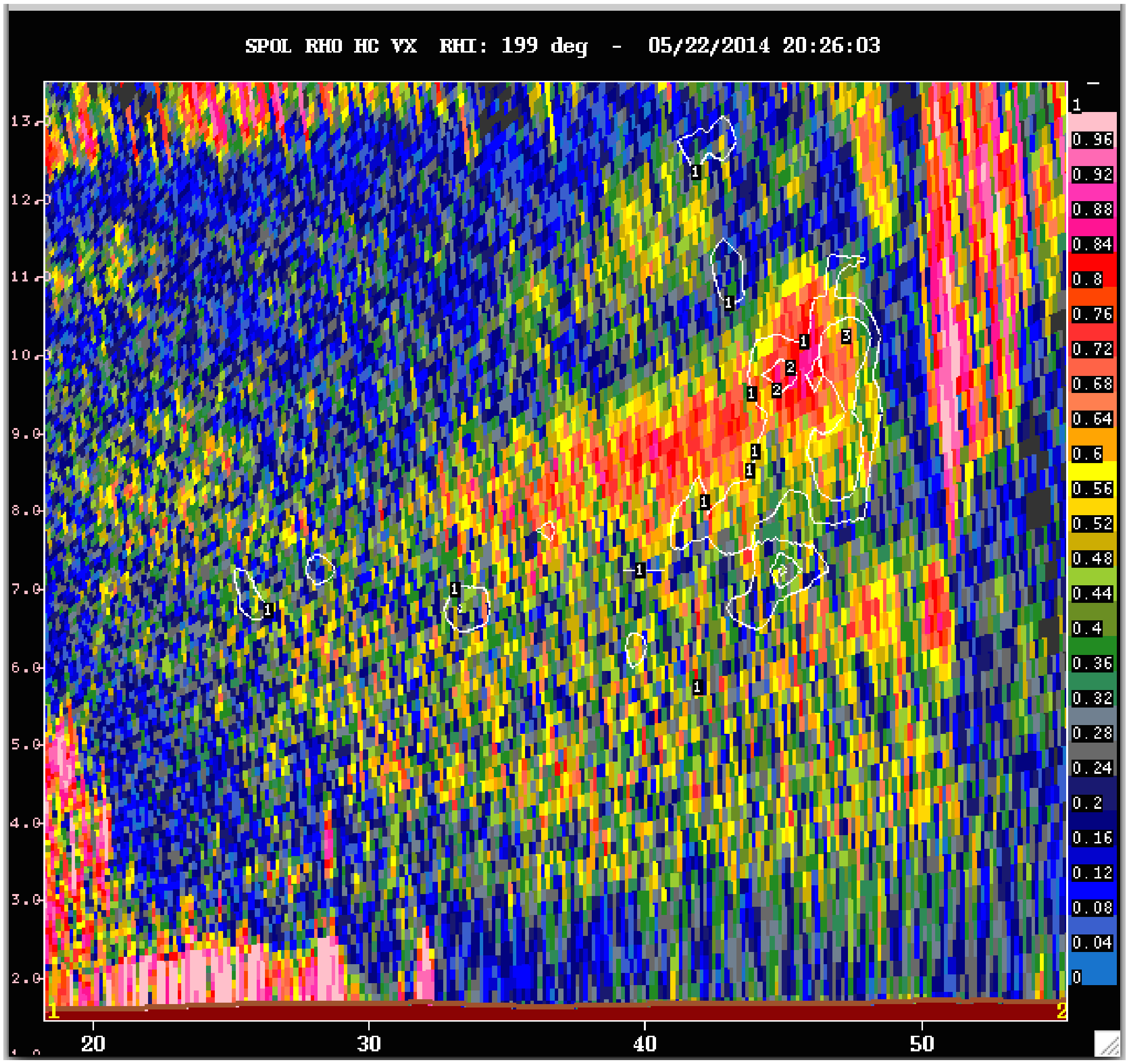

Figure 17: *An RHI of S-Pol co-to-cross correlation coefficient, ρ_x, accompanying Fig. 15.*